ACS APPLIED MATERIALS & INTERFACES

Research Article

www.acsami.org

Simple O_2 Plasma-Processed V_2O_5 as an Anode Buffer Layer for High-Performance Polymer Solar Cells

Xichang Bao,[†] Qianqian Zhu,[‡] Ting Wang,[†] Jing Guo,[†] Chunpeng Yang,[†] Donghong Yu,[§,∥] Ning Wang,[†] Weichao Chen,[†] and Renqiang Yang*[,†,⊥]

[†]CAS Key Laboratory of Bio-based Materials, Qingdao Institute of Bioenergy and Bioprocess Technology, Chinese Academy of Sciences, Qingdao 266101, China

[‡]College of Materials Science and Engineering, Qingdao University of Science and Technology, Qingdao 266042, China

[§]Department of Chemistry and Bioscience, Aalborg University, DK-9220 Aalborg, Denmark

[∥]Sino-Danish Centre for Education and Research (SDC), Niels Jenses Vej 2, DK-8000 Aarhus, Denmark

[⊥]State Key Laboratory of Luminescent Materials and Devices, South China University of Technology, Guangzhou 510641, China

Supporting Information

ABSTRACT: A simple O_2 plasma processing method for preparation of a vanadium oxide (V_2O_5) anode buffer layer on indium tin oxide (ITO)-coated glass for polymer solar cells (PSCs) is reported. The V_2O_5 layer with high transmittance and good electrical and interfacial properties was prepared by spin coating a vanadium(V) triisopropoxide oxide alcohol solution on ITO and then O_2 plasma treatment for 10 min [V_2O_5 (O_2 plasma)]. PSCs based on P3HT:$PC_{61}BM$ and PBDTTT-C:$PC_{71}BM$ using V_2O_5 (O_2 plasma) as an anode buffer layer show high power conversion efficiencies (PCEs) of 4.47 and 7.54%, respectively, under the illumination of AM 1.5G (100 mW/cm^2). Compared to that of the control device with PBDTTT-C:$PC_{71}BM$ as the active layer and PEDOT:PSS (PCE of 6.52%) and thermally annealed V_2O_5 (PCE of 6.27%) as the anode buffer layer, the PCE was improved by 15.6 and 20.2%, respectively, after the introduction of a V_2O_5 (O_2 plasma) anode buffer layer. The improved PCE is ascribed to the greatly improved fill factor and enhanced short-circuit current density of the devices, which benefited from the change in the work function of V_2O_5, a surface with many dangling bonds for better interfacial contact, and the excellent charge transport property of the V_2O_5 (O_2 plasma) layer. The results indicate that an O_2 plasma-processed V_2O_5 film is an efficient and economical anode buffer layer for high-performance PSCs. It also provides an attractive choice for low-cost fabrication of organic electronics.

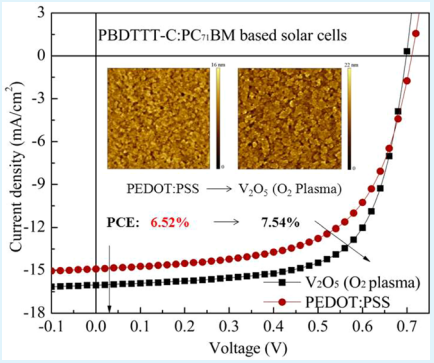

KEYWORDS: *efficient polymer solar cells, O_2 plasma processing, V_2O_5, anode buffer layer, annealing-free*

1. INTRODUCTION

Over the past few decades, polymer solar cells (PSCs) have attracted a great deal of attention because of their low cost, light weight, and ease of use for large-area manufacturing on flexible substrates.[1−4] Recently, there have been great advances in PSCs, and the power conversion efficiencies (PCEs) of bulk heterojunction (BHJ) PSCs are >9%[5,6] and >10%[7] for single-junction and tandem structures, respectively. However, as shown by the research focused on considerate tailoring of the molecular structures of active materials[8−11] and optimization of the active layer morphology,[11−13] the suitable interfaces between the two contact electrodes and the photoactive layer are very important for the improvement of the efficiency and long-term stability of the solar cells. The effective interfacial layer can form ohmic contacts, which can effectively collect and transport charges at the interfaces. For conventional devices with indium tin oxide (ITO) as the anode, polyethylenedioxythiophene:polystyrenesulfonate (PEDOT:PSS) is the most widely used anode buffer layer in organic solar cells. However, the strong acidic nature and hygroscopic properties of PEDOT:PSS could induce the degradation of the stability of the PSCs.[12−14] The device performance and stability can be improved through introduction of other air-stable interfacial materials. In recent years, conductive conjugated polymers,[15,16] graphene oxide,[17,18] NiAc,[19] transition metal oxides (MoO_3, NiO, WO_3, ReO_x, and V_2O_5),[20−35] and developing a new method[36] have attracted attention. Among the transition metal oxides, especially, V_2O_5 is an effective anode buffer layer in PSCs.[25−35] It is a very promising material because of its suitable optical and electrical properties, high work function, ambient stability, and ability to minimize the contact resistance. Most of the previous works have focused on vacuum thermally evaporated V_2O_5 as the anode buffer layer used in conventional or inverted devices.[25−28] However, the vacuum thermal evaporation technique could have some drawbacks for applications in organic solar cells, such as cost and

Received: January 5, 2015
Accepted: March 26, 2015
Published: March 26, 2015

DOI: 10.1021/acsami.5b00091
ACS Appl. Mater. Interfaces 2015, 7, 7613−7618

incompatibility with the easy processing of PSCs. There are some reports using solution-processed V_2O_5 as an anode buffer layer to improve device performance. Huang et al. reported that solution-processed V_2O_5 for PSCs as the anode buffer layer by using V_2O_5 powder suspended in 2-propanol.[29] Unfortunately, the device shows poor performance because the film exists as small islands. Recently, vanadium(V) triisopropoxide oxide was proven to be a good precursor for solution-processed V_2O_5 as an anode buffer layer in PSCs.[31−35] The reported V_2O_5 was obtained by the precursor reacted with water or hydrolysis under ambient conditions for a long time. However, the devices show a relatively low fill factor (FF of ∼60%) because of the poor interfacial contact.

To improve the interfacial properties and simplify the preparation process of V_2O_5, a simple O_2 plasma processing method was introduced. The smooth V_2O_5 layer was prepared by spin coating a vanadium(V) triisopropoxide oxide alcohol solution and then treated with O_2 plasma [V_2O_5 (O_2 plasma)]. The precursor can be decomposed to V_2O_5 by O_2 plasma without the need for hydrolysis with moisture. The surface contains a large quantity of dangling bonds, which could facilitate the formation of an excellent interfacial contact. Hence, the FF was greatly improved when using V_2O_5 (O_2 plasma) as the anode buffer layer in the poly(3-hexylthiophene):[6,6]-phenyl-C61-butyric acid methyl ester (P3HT:PC_{61}BM, 73.55%)-based and poly(4,8-bis-alkyloxybenzo[1,2-b:4,5-b′]dithiophene-*alt*-alkylcarbonyl-thieno[3,4-*b*]thiophene):[6,6]-phenyl-C71-butyric acid methyl ester (PBDTTT-C:PC_{71}BM, 67.33%)-based solar cells. In comparison with the control device using PBDTTT-C:PC_{71}BM as the active layer and PEDOT:PSS (PCE of 6.52%) and thermally annealed V_2O_5 (PCE of 6.27%) as anode buffer layers, the PCE was improved by 15.6 and 20.2%, respectively, via the introduction of O_2 plasma-processed V_2O_5 as the anode buffer layer (PCE of 7.54%).

2. EXPERIMENTAL SECTION

2.1. Materials. ITO-coated glass with a sheet resistance of 15 Ω/sq was obtained from Shenzhen Display Corp. Vanadium(V) triisopropoxide oxide was purchased from Alfa Aesar. PEDOT:PSS (Clevious P VP AI 4083) was obtained from H. C. Stark. P3HT and PBDTTT-C were bought from Lumtec and Solarmer, respectively. PC_{61}BM and PC_{71}BM were supplied by American Dye Sources (ADS). 1,8-Diiodooctane (DIO) was supplied by Sigma-Aldrich. All commercial materials were used directly.

2.2. V_2O_5 and Device Fabrication. Several conventional PSCs (devices A−E) were fabricated, and the device structures were as follows: (A) ITO/V_2O_5 (O_2 plasma, 14 nm)/P3HT:PC_{61}BM (200 nm)/Ca (10 nm)/Al (100 nm), (B) ITO/V_2O_5 (annealed, 14 nm)/P3HT:PC_{61}BM (200 nm)/Ca (10 nm)/Al (100 nm), (C) ITO/PEDOT:PSS (30 nm)/P3HT:PC_{61}BM (200 nm)/Ca (10 nm)/Al (100 nm), (D) ITO/V_2O_5 (O_2 plasma, 14 nm)/PBDTTT-C:PC_{71}BM (90 nm)/Ca (10 nm)/Al (100 nm), (E) ITO/V_2O_5 (annealed, 14 nm)/PBDTTT-C:PC_{71}BM (90 nm)/Ca (10 nm)/Al (100 nm), and (F) ITO/PEDOT:PSS (30 nm)/PBDTTT-C:PC_{71}BM (90 nm)/Ca (10 nm)/Al (100 nm). ITO-coated glass was sequentially ultrasonically washed in detergent, deionized water, acetone, and 2-propanol for 20 min each. Afterward, the precleaned ITO-coated glass was exposed to oxygen plasma to remove organic contaminants and increase the size of the wetting envelope. The V_2O_5 layer was obtained by spin coating a vanadium(V) triisopropoxide oxide alcohol solution [2% (v/v)] at 4000 rpm on precleaned ITO substrates and then treated under O_2 plasma [V_2O_5 (O_2 plasma)] for 10 min without the need for hydrolysis with moisture or annealed at 150 °C for 30 min [V_2O_5 (annealed)]. PEDOT:PSS films were prepared by spin coating its aqueous solution on ITO-coated glass at 4000 rpm for 30 s and then thermally annealed at 150 °C for 30 min. Subsequently, the modified ITO-coated glass was moved to the glovebox. For P3HT:PC_{61}BM-based devices, the active layer was prepared by spin coating the chlorobenzene solution of P3HT and PC_{61}BM [1:1 (w/w), total concentration of 36 mg/mL] on the modified ITO electrode and then thermally annealed at 150 °C for 10 min on a hot plate. For the PBDTTT-C:PC_{71}BM-based solar cells, the active layer was obtained by spin coating the dichlorobenzene solution of PBDTTT-C and PC_{71}BM [1:1.5 (w/w), total concentration of 31 mg/mL] with a 3% volume ratio of DIO additive on the modified ITO substrates. Finally, the Ca (10 nm)/Al (100 nm) bilayer cathode was thermally deposited. The device area was 0.1 cm^2 defined by a shadow mask.

2.3. Measurements. The grazing incidence X-ray diffraction (GIXRD) result was achieved with a Bruker D8 ADVANCE instrument. An ESCA Lab250i-XL electron spectrometer (Thermo, 150 W Al Kα radiation) was used to obtain X-ray photoelectron spectroscopy (XPS) results. The transmission spectra of the films were observed by a scanning spectrophotometer (Varian Cary 50 UV/vis). Surface morphologies of the films were characterized by an Agilent 5400 atomic force microscope (AFM). The water contact angle results were obtained on a homemade JY-82 contact angle system (China). The deionized water was obtained from a Millipore ultrapure water system. The thickness of the layer was determined with a Dektak 150 profilometer. Current density−voltage (J−V) curves were measured with a Keithley 2420 source measurement unit under the illumination of AM 1.5G (100 mW/cm^2) with a Newport solar simulator.

3. RESULTS AND DISCUSSION

3.1. Characterization of the V_2O_5 Layer. To determine the purity and composition of the prepared anode buffer layers, XPS measurements were taken. The samples were fabricated through spin coating a vanadium(V) triisopropoxide oxide alcohol solution [2% (v/v)] at 4000 rpm on the precleaned silicon substrate and then treated as the devices were prepared. The results are shown in Figure 1. The binding energies (BEs)

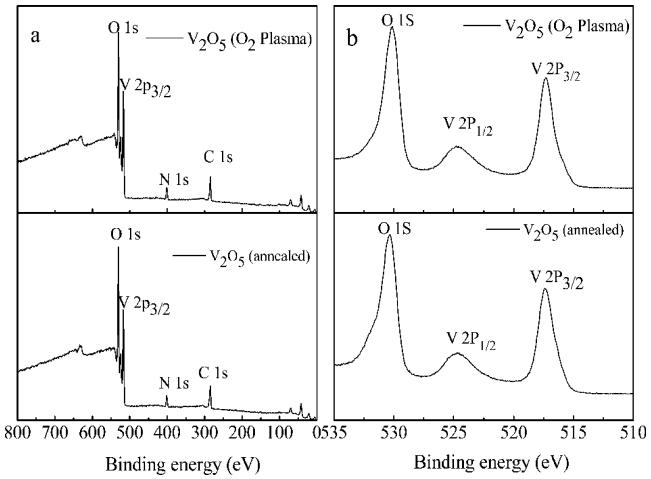

Figure 1. XPS spectra of the V_2O_5 layer: (a) survey scan and (b) V 2p and O 1s core-level spectra.

are corrected with C 1s (284.42 eV). As presented in Figure 1a, there are characteristic peaks of V, O, C, and N elements in the 0−800 eV BE range. For the V_2O_5 layer prepared with O_2 plasma, the peaks are for V 2p at 517.32 eV, O 1s at 530.22 eV, and N 1s at 401.42 eV. Interestingly, the peaks for the annealed V_2O_5 layer are the same as those for the V_2O_5 layer prepared with O_2 plasma. In Figure 1b, there are two vanadium peaks that correspond to a doublet of V $2p_{3/2}$ (∼517.32 eV) and V $2p_{1/2}$ (∼524.77 eV) for an O_2 plasma prepared layer and V

DOI: 10.1021/acsami.5b00091
ACS Appl. Mater. Interfaces 2015, 7, 7613−7618

$2p_{3/2}$ (~517.42 eV) and V $2p_{1/2}$ (~524.72 eV) for an annealed V_2O_5 film, in which one is the $^3/_2$ and the other the $^1/_2$ spin–orbit split component. The narrow V $2p_{3/2}$ peaks (517.32 and 517.42 eV) for the two samples are very close to the reported one for crystalline V_2O_5 (517.2 eV).[37] The O 1s core level of XPS spectra has one strong peak at ~530.22 eV for both samples, which can be assigned to the oxygen atoms in stoichiometric V_2O_5. The XPS results confirm that vanadium(V) triisopropoxide oxide is decomposed into V_2O_5 completely after the O_2 plasma is processed or thermally annealed at 150 °C for 30 min.

The transmittance spectra of the V_2O_5 films, PEDOT:PSS on ITO-coated glass, and bare ITO-coated glass are shown in Figure 2. For the control PEDOT:PSS-modified ITO-coated glass, the antireflective effect in the wavelength range of 330–410 nm was ascribed to the smooth surface, which will be discussed below. The smooth surface could reduce the level of dispersion and extinction of light.[38] Furthermore, the obtained V_2O_5 films prepared by different methods also have good transmittance in the visible range, and their transmittance spectra are almost the same. The good transmittance is helpful for obtaining high-performance PSCs.

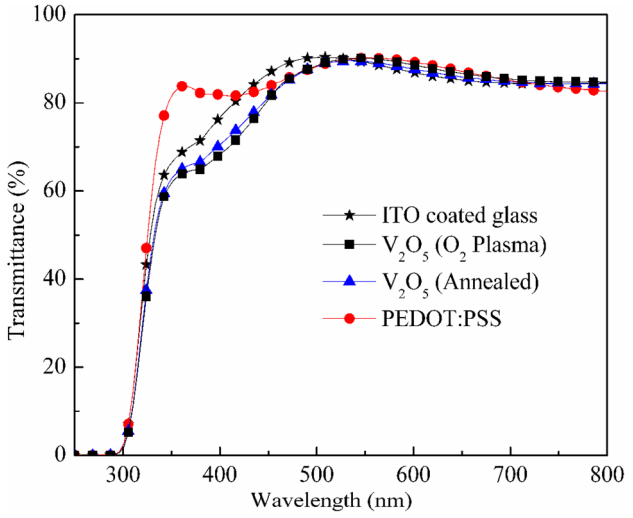

Figure 2. Optical transmittance of bare ITO-coated glass, the V_2O_5 layer, and PEDOT:PSS-modified ITO-coated glass.

3.2. Photovoltaic Performance of the PSCs. To investigate the effect of the V_2O_5 (O_2 plasma) as an anode buffer layer on the photovoltaic performance of the PSCs, several kinds of devices were fabricated as mentioned above. Figure 3 illustrates the current density–voltage (J–V) characteristics of the PSCs with different anode buffer layers under the illumination of AM 1.5G (100 mW/cm^2). The optimized device performance and the average PCEs of 10 different devices are listed in Table 1. For P3HT:PC_{61}BM-based solar cells, device C with a traditional PEDOT:PSS anode buffer layer gives a PCE of 3.92% with an open-circuit voltage (V_{OC}) of 0.64 V, a short-circuit current density (J_{SC}) of 9.21 mA/cm^2, and an FF of 66.17%. Device B with a V_2O_5 (annealed) anode buffer layer gives a PCE of 3.64% with a V_{OC} of 0.62 V, a J_{SC} of 9.20 mA/cm^2, and an FF of 64.15%. This value is consistent with V_2O_5 as the anode buffer layer prepared with vanadium(V) triisopropoxide oxide reported elsewhere.[31,32] In comparison, the J_{SC} and best PCE of device A with a V_2O_5 (O_2 plasma) anode buffer layer are enhanced to

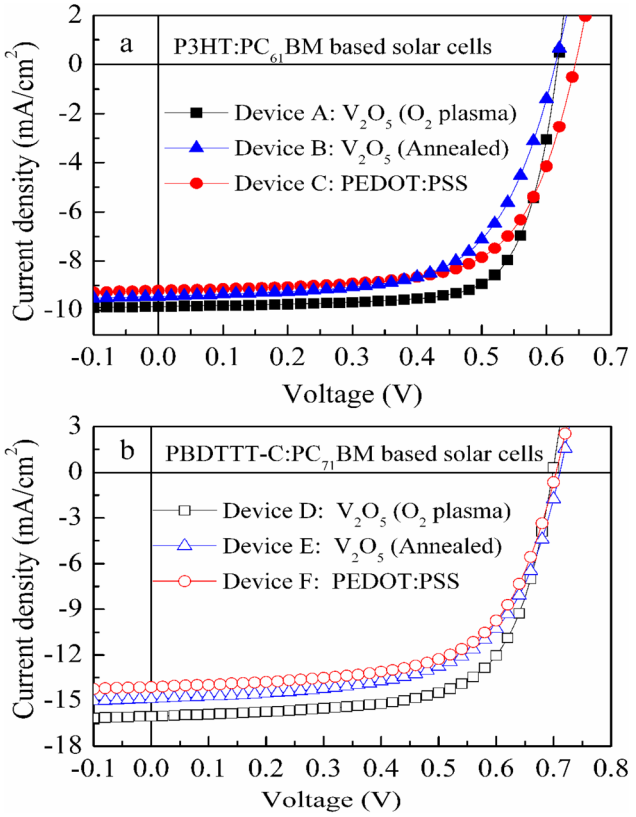

Figure 3. J–V curves of the PSCs with different anode buffer layers: (a) P3HT:PC_{61}BM and (b) PBDTTT-C:PC_{71}BM.

9.84 mA/cm^2 and 4.47%, respectively. Most importantly, the FF has been remarkably improved to 73.55%, which is one of the highest values of the P3HT:PC_{61}BM-based devices. Furthermore, P3HT:PC_{61}BM solar cells with different thicknesses of the V_2O_5 layer prepared by O_2 plasma were also fabricated (Figure S1 and Table S1 of the Supporting Information). All devices exhibit good performance with high FF values of >70%.

To further explore the general applicability of the V_2O_5 anode buffer layer in the PSCs, another typical efficient low bandgap polymer, PBDTTT-C, was used as a donor. The J–V curves of the PBDTTT-C:PC_{71}BM-based solar cells are shown in Figure 3b, and their related device performance parameters are also included in Table 1. The traditional control device F with PEDOT:PSS as anode buffer layer exhibits a PCE of 6.52% with a V_{OC} of 0.71 V, a J_{SC} of 14.90 mA/cm^2, and an FF of 61.65%, which are consistent with those previously reported.[39,40] The device with a V_2O_5 (O_2 plasma) anode buffer layer shows a high PCE of 7.54% with a V_{OC} of 0.70 V, a J_{SC} of 16.03 mA/cm^2, and an FF of 67.33%, and the average PCE of 10 devices is 7.41%. The champion and average PCEs both are one of the highest values for the PBDTTT-C:PC_{71}BM-based devices. In contrast, another control device E with a V_2O_5 (annealed) anode buffer layer was also prepared and shows a PCE of 6.27% with a V_{OC} of 0.70 V, a J_{SC} of 14.11 mA/cm^2, and an FF of 63.26%. According to a previous report, the work function of the solution-processed V_2O_5 layer is 5.10 eV, which is lower (0.34 eV) than the highest occupied molecular orbital (HOMO) of P3HT. The holes can be easily transferred from the HOMO level of P3HT to the V_2O_5 layer and collected with an ITO electrode.[30,33] Furthermore, the

DOI: 10.1021/acsami.5b00091
ACS Appl. Mater. Interfaces 2015, 7, 7613–7618

Table 1. Device Performance of the PSCs with Different Anode Buffer Layers

device	hole transport layer	active layer	V_{OC} (V)	J_{SC} (mA/cm^2)	FF (%)	maximal PCE (%)	average PCE (%)	calcd J_{SC} (mA/cm^2)
A	V_2O_5 (O_2 plasma)	P3HT:$PC_{61}BM$	0.62	9.84	73.55	4.47	4.29	9.31
B	V_2O_5 (annealed)	P3HT:$PC_{61}BM$	0.62	9.20	64.15	3.64	3.53	8.83
C	PEDOT:PSS	P3HT:$PC_{61}BM$	0.64	9.21	66.17	3.92	3.81	8.74
D	V_2O_5 (O_2 plasma)	PBDTTT-C:$PC_{71}BM$	0.70	16.03	67.33	7.54	7.41	15.07
E	V_2O_5 (annealed)	PBDTTT-C:$PC_{71}BM$	0.70	14.11	63.26	6.27	5.96	13.21
F	PEDOT:PSS	PBDTTT-C:$PC_{71}BM$	0.71	14.90	61.65	6.52	6.38	13.89

work function can be increased by O_2 treatment.[41] Thus, the device could exhibit improved performance. Moreover, the improved PCE and FF of V_2O_5 (O_2 plasma)-modified devices could be due to improved charge transport properties of the V_2O_5 layer and enhanced charge collection at the V_2O_5–donor interface.

Furthermore, the corresponding external quantum efficiencies (EQEs) of the solar cells with different anode buffer layers were measured to verify the accuracy of the J–V results. The spectra are shown in Figure S2 of the Supporting Information. The EQE results agree well with the J_{SC}. Especially for PBDTTT-C:$PC_{71}BM$ solar cells, the maximal EQE reached 68.48% at 660 nm for the device with a V_2O_5 (O_2 plasma) anode buffer layer, and these cells show a much better photoresponse in the broad range of 430–710 nm. Moreover, the calculated J_{SC} values determined via integration of the spectral response of the solar cells are also shown in Table 1. The J_{SC} values are consistent with the J_{SC} values obtained from the J–V curves. These results again indicate that the V_2O_5 (O_2 plasma) anode buffer layer is helpful for improving the device performance.

Figure 4 shows the surface morphology of the bare ITO substrate, control PEDOT:PSS, and V_2O_5-modified ITO-coated glass observed by tapping-mode atomic force microscopy. The root-mean-square (rms) value of the bare ITO-coated glass was 4.04 nm. When modified by V_2O_5 films, the surface became smooth, and the rms values were almost the same (2.31 nm for the O_2 plasma film and 2.24 nm for the annealed film), which are comparable with that of the PEDOT:PSS-modified ITO-coated glass (1.68 nm). Moreover,

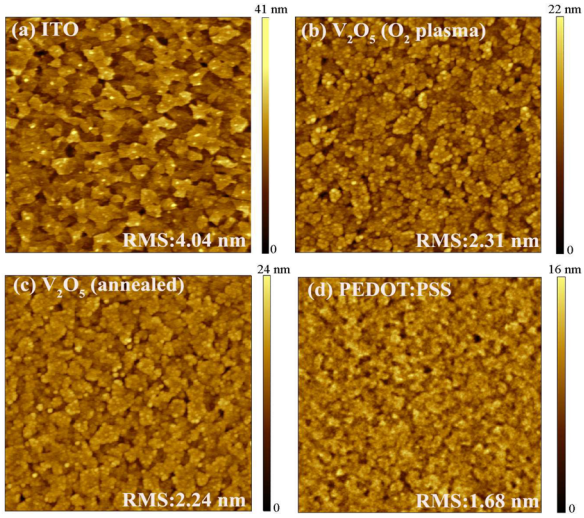

Figure 4. Tapping-mode AFM height images of (a) bare ITO-coated glass, (b) the V_2O_5 (O_2 plasma) layer, (c) the V_2O_5 (annealed) layer, and (d) the control PEDOT:PSS layer. The scan size is 5 μm × 5 μm.

the surface morphologies of P3HT:$PC_{61}BM$ active layers on different anode buffer layers were measured as shown in Figure S3 of the Supporting Information. The surfaces are very smooth without obvious differences. The lack of significant changes in surface morphology of active layers and different anode buffer layer indicates that the rms value is not the determinant factor in the variations of device performance. However, from panels b and c of Figure 4, the V_2O_5 (O_2 plasma) layer shows an interface much clearer than that of the V_2O_5 (annealed) layer, which could be ascribed to the reduction of residual organic contamination on the surface after O_2 plasma treatment. This could increase the work function of the V_2O_5 layer.[42,43] Concomitantly, the PCE and FF were improved for the devices fabricated on the top of V_2O_5 (O_2 plasma). Furthermore, the surface of the V_2O_5 (O_2 plasma) layer could form many dangling bonds because of the preparation process.[44] These dangling bonds are quite unstable, and surface reconstruction occurs substantially, which would form a better interfacial contact. To further confirm this hypothesis, the surface energy of the V_2O_5 layer was studied by contact angle measurements as shown in Figure 5. For

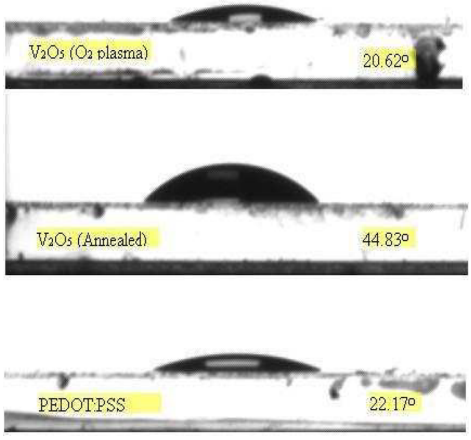

Figure 5. Measured water contact angle between a drop of deionized water and the anode buffer layer. V_2O_5 (O_2 plasma), V_2O_5 (annealed), and PEDOT:PSS layers from top to bottom, respectively.

comparison, the contact angle of the PEDOT:PSS layer was also measured, and the result is 22.17°. As shown in Figure 5, the contact angle for the V_2O_5 (O_2 plasma) layer is only 20.62°; however, the contact angle of the V_2O_5 (annealed) layer is increased to 44.83°. The results show that the V_2O_5 (O_2 plasma) layer exhibits better interface properties when the active layer was spin coated onto it. We can conclude that the better contact properties and many of the surface dangling bonds are the main reasons for the improved performance of the solar cell with the V_2O_5 (O_2 plasma) layer as the anode buffer layer.

DOI: 10.1021/acsami.5b00091
ACS Appl. Mater. Interfaces 2015, 7, 7613–7618

Furthermore, the electrical properties of the different anode buffer layers as the optimized solar cells used were investigated using a simple Ohm's law with the shadow mask as the solar cell preparation, and the results are shown in Figure 6; the

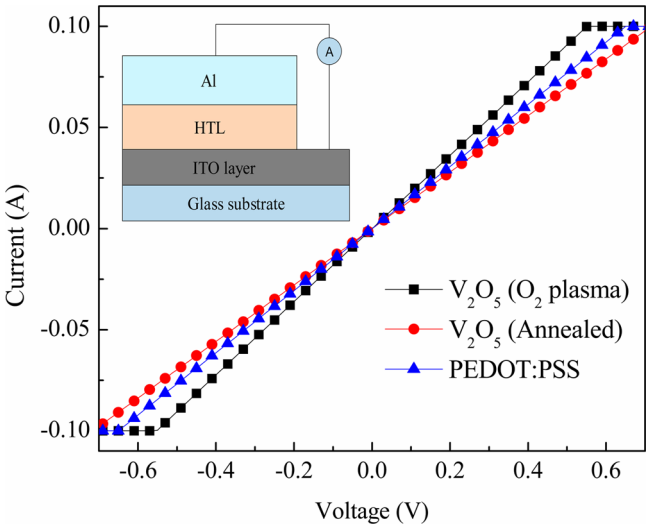

Figure 6. Current–voltage characteristics of different anode buffer layers.

schematic structure of the measurement is included as the inset. Interestingly, the *I*–*V* curve of the V_2O_5 (O_2 plasma) layer exhibits the greatest slope among the three anode buffer layers. By contrast, the V_2O_5 (annealed) layer shows the smallest slope with the largest resistance. The resistances are 5.45, 6.52, and 7.15 Ω for V_2O_5 (O_2 plasma), PEDOT:PSS, and V_2O_5 (annealed), respectively. The better electrical transport property of the V_2O_5 (O_2 plasma) layer is another reason for the improved solar cell performance.

4. CONCLUSION

In summary, annealing-free V_2O_5 films were obtained by spin coating a vanadium(V) triisopropoxide oxide alcohol solution on the ITO-coated glass and treated with O_2 plasma for 10 min [V_2O_5 (O_2 plasma)]. The V_2O_5 layer shows good optical transmittance and electrical properties. PSCs based on P3HT:PC_{61}BM and PBDTTT-C:PC_{71}BM using a V_2O_5 (O_2 plasma) anode buffer layer show high PCEs of 4.47 and 7.54%, respectively, under the illumination of AM 1.5G (100 mW/cm^2), which are increased by 14.0 and 15.6%, respectively, in comparison with those of the devices with a conventional PEDOT:PSS layer (3.92 and 6.52%, respectively). Compared to that of the solar cell with a V_2O_5 (annealed) anode buffer layer and PBDTTT-C:PC_{71}BM as an active layer (PCE of 6.27%), the PCE was improved by 20.2% through greatly improved values of FF and J_{SC} upon introduction of V_2O_5 (O_2 plasma) as an anode buffer layer. The improved device performance is ascribed to the modified surface with an improved work function, the presence of many dangling bonds for better interface contact, and the excellent electrical transport property of V_2O_5 (O_2 plasma). The results indicate that an O_2 plasma-processed V_2O_5 film is an efficient and economical anode buffer layer for high-performance PSCs. It also provides an attractive alternative for low-cost fabrication of organic electronics.

■ ASSOCIATED CONTENT

Supporting Information

J–*V* curves of P3HT:PC_{61}BM solar cells with different V_2O_5 (O_2 plasma) thicknesses, EQE curves of the PSCs with different anode buffer layers, and AFM images of P3HT:PC_{61}BM on different buffer layers. This material is available free of charge via the Internet at http://pubs.acs.org.

■ AUTHOR INFORMATION

Corresponding Author

*E-mail: yangrq@qibebt.ac.cn.

Notes

The authors declare no competing financial interest.

■ ACKNOWLEDGMENTS

This work was supported by the National Natural Science Foundation of China (61107090, 61405209, 51303197, 51173199, and 21204097), the Ministry of Science and Technology of China (2014CB643501 and 2010DFA52310), and the Qingdao Municipal Science and Technology Program (11-2-4-22-hz and 14-2-4-28-jch). Support from the Sino-Danish Centre for Education and Research (SDC) is also fully acknowledged.

■ REFERENCES

(1) Blom, P.; Mihailetchi, V.; Koster, L.; Markov, D. Device Physics of Polymer:Fullerene Bulk Heterojunction Solar Cells. *Adv. Mater. (Weinheim, Ger.)* **2007**, *19*, 1551–1566.

(2) Krebs, F. Polymer Solar Cell Modules Prepared using Roll-to-Roll Methods: Knife-Over-Edge Coating, Slot-die Coating and Screen Printing. *Sol. Energy Mater. Sol. Cells* **2009**, *93*, 465–475.

(3) Krebs, F.; Jørgensen, M.; Norrman, K.; Hagemann, O.; Alstrup, J.; Nielsen, T.; Fyenbo, J.; Larsen, K.; Kristensen, A. J. Complete Process for Production of Flexible Large Area Polymer Solar Cells Entirely using Screen Printing-First Public Demonstration. *Sol. Energy Mater. Sol. Cells* **2009**, *93*, 422–441.

(4) Li, G.; Shrotriya, V.; Huang, J.; Yao, Y.; Moriarty, T.; Emery, K.; Yang, Y. High-Efficiency Solution Processable Polymer Photovoltaic Cells by Self-Organization of Polymer Blends. *Nat. Mater.* **2005**, *4*, 864–868.

(5) He, Z.; Zhong, C.; Su, S.; Xu, M.; Wu, H.; Cao, Y. Enhanced Power-conversion Efficiency in Polymer Solar Cells using an Inverted Device Structure. *Nat. Photonics* **2012**, *6*, 591–595.

(6) Liao, S.; Jhuo, H.; Cheng, Y.; Chen, S. Fullerene Derivative-Doped Zinc Oxide Nanofilm as the Cathode of Inverted Polymer Solar Cells with Low-Bandgap Polymer (PTB7-Th) for High Performance. *Adv. Mater. (Weinheim, Ger.)* **2013**, *25*, 4766–4771.

(7) You, J.; Chen, C. C.; Hong, Z.; Yoshimura, K.; Ohya, K.; Xu, R.; Ye, S.; Gao, J.; Li, G.; Yang, Y. 10.2% Power Conversion Efficiency Polymer Tandem Solar Cells Consisting of Two Identical Sub-Cells. *Adv. Mater. (Weinheim, Ger.)* **2013**, *25*, 3973–3978.

(8) Price, S.; Stuart, A.; Yang, L.; Zhou, H.; You, W. Fluorine Substituted Conjugated Polymer of Medium Band Gap Yields 7% Efficiency in Polymer–Fullerene Solar Cells. *J. Am. Chem. Soc.* **2011**, *133*, 4625–4631.

(9) Zhang, M.; Guo, X.; Zhang, S.; Hou, J. Synergistic Effect of Fluorination on Molecular Energy Level Modulation in Highly Efficient Photovoltaic Polymer. *Adv. Mater. (Weinheim, Ger.)* **2014**, *26*, 1118–1123.

(10) Ye, L.; Zhang, S.; Huo, L.; Zhang, M.; Hou, J. Molecular Design toward Highly Efficient Photovoltaic Polymers Based on Two-Dimensional Conjugated Benzodithiophene. *Acc. Chem. Res.* **2014**, *47*, 1595–1603.

(11) Li, W.; Roelofs, W. S.; Wienk, M.; Janssen, R. Enhancing the Photocurrent in Diketopyrrolopyrrole-Based Polymer Solar Cells via Energy Level Control. *J. Am. Chem. Soc.* **2012**, *134*, 13787–13795.

DOI: 10.1021/acsami.5b00091
ACS Appl. Mater. Interfaces 2015, 7, 7613–7618

(12) Jorgensen, M.; Norrman, K.; Krebs, F. Stability/Degradation of Polymer Solar Cells. *Sol. Energy Mater. Sol. Cells* **2008**, *92*, 686−714.
(13) Paci, B.; Generosi, A.; Albertini, V.; Perfetti, P.; Bettignies, R.; Sentein, C. Time-resolved Morphological Study of Organic Thin Film Solar Cells based on Calcium/Aluminium Cathode Material. *Chem. Phys. Lett.* **2008**, *461*, 77.
(14) Norrman, K.; Gevorgyan, S.; Krebs, F. Water-Induced Degradation of Polymer Solar Cells Studied by $H_2{}^{18}O$ Labeling. *ACS Appl. Mater. Interfaces* **2009**, *1*, 102−112.
(15) Shelton, S.; Chen, T.; Barclay, D.; Ma, B. Solution-Processable Triindoles as Hole Selective Materials in Organic Solar Cells. *ACS Appl. Mater. Interfaces* **2012**, *4*, 2534−2540.
(16) Jung, J. W.; Lee, J. U.; Jo, W. H. High-Efficiency Polymer Solar Cells with Water-Soluble and Self-Doped Conducting Polyaniline Graft Copolymer as Hole Transport Layer. *J. Phys. Chem. C* **2010**, *114*, 633−637.
(17) Li, S.; Tu, K.; Lin, C.; Chen, C.; Chhowalla, M. Solution-Processable Graphene Oxide as an Efficient Hole Transport Layer in Polymer Solar Cells. *ACS Nano* **2010**, *4*, 3169−3174.
(18) Liu, J.; Kim, G.; Xue, Y.; Kim, J.; Baek, J.; Durstock, M.; Dai, L. Graphene Oxide Nanoribbon as Hole Extraction Layer to Enhance Efficiency and Stability of Polymer Solar Cells. *Adv. Mater. (Weinheim, Ger.)* **2014**, *26*, 786−790.
(19) Tan, Z.; Zhang, W.; Qian, D.; Cui, C.; Xu, Q.; Li, L.; Li, S.; Li, Y. Solution-Processed Nickel Acetate as Hole Collection Layer for Polymer Solar Cells. *Phys. Chem. Chem. Phys.* **2012**, *14*, 14217−14223.
(20) Li, X.; Choy, W.; Xie, F.; Zhang, S.; Hou, J. Room-Temperature Solution-Processed Molybdenum Oxide as a Hole Transport Layer with Ag Nanoparticles for Highly Efficient Inverted Organic Solar Cells. *J. Mater. Chem. A* **2013**, *1*, 6614−6621.
(21) Tan, Z.; Qian, D.; Zhang, W.; Li, L.; Ding, Y.; Xu, Q.; Wang, F.; Li, Y. Efficient and Stable Polymer Solar Cells with Solution-Processed Molybdenum Oxide Interfacial Layer. *J. Mater. Chem. A* **2013**, *1*, 657−664.
(22) Steirer, K.; Ndione, P.; Widjonarko, N.; Lloyd, M.; Meyer, J.; Ratcliff, E.; Kahn, A.; Armstrong, N.; Curtis, C.; Ginley, D.; Berry, J.; Olson, D. Enhanced Efficiency in Plastic Solar Cells via Energy Matched Solution Processed NiO_x Interlayers. *Adv. Energy Mater.* **2011**, *1*, 813−820.
(23) Tan, Z.; Li, L.; Cui, C.; Ding, Y.; Xu, Q.; Li, S.; Qian, D.; Li, Y. Solution-Processed Tungsten Oxide as an Effective Anode Buffer Layer for High-Performance Polymer Solar Cells. *J. Phys. Chem. C* **2012**, *116*, 18626−18632.
(24) Tan, Z.; Li, L.; Wang, F.; Xu, Q.; Li, S.; Sun, G.; Tu, X.; Hou, X.; Hou, J.; Li, Y. Solution-Processed Rhenium Oxide: A Versatile Anode Buffer Layer for High Performance Polymer Solar Cells with Enhanced Light Harvest. *Adv. Energy Mater.* **2014**, *4*, 1300884.
(25) Shrotriya, V.; Li, G.; Yao, Y.; Chu, C.; Yang, Y. Transition Metal Oxides as the Buffer Layer for Polymer Photovoltaic Cells. *Appl. Phys. Lett.* **2006**, *88*, 073508.
(26) Liao, H.; Chen, L.; Xu, Z.; Li, G.; Yang, Y. Highly Efficient Inverted Polymer Solar Cell by Low Temperature Annealing of Cs_2CO_3 Interlayer. *Appl. Phys. Lett.* **2008**, *92*, 173303.
(27) Takanezawa, K.; Tajima, K.; Hashimoto, K. Efficiency Enhancement of Polymer Photovoltaic Devices Hybridized with ZnO Nanorod Arrays by the Introduction of a Vanadium Oxide Buffer Layer. *Appl. Phys. Lett.* **2008**, *93*, 063308.
(28) Shen, L.; Xu, Y.; Meng, F.; Li, F.; Ruan, S.; Chen, W. SemiTransparent Polymer Solar Cells using $V_2O_5/Ag/V_2O_5$ as Transparent Anodes. *Org. Electron.* **2011**, *12*, 1223−1226.
(29) Huang, J.; Chou, C.; Liu, M.; Tsai, K.; Lin, W.; Lin, C. Solution-Processed Vanadium Oxide as an Anode Interlayer for Inverted Polymer Solar Cells Hybridized with ZnO Nanorods. *Org. Electron.* **2009**, *10*, 1060−1065.
(30) Tan, Z.; Zhang, W.; Cui, C.; Ding, Y.; Qian, D.; Xu, Q.; Li, L.; Li, S.; Li, Y. Solution-Processed Vanadium Oxide as a Hole Collection Layer on an ITO Electrode for High-Performance Polymer Solar Cells. *Phys. Chem. Chem. Phys.* **2012**, *14*, 14589−14595.
(31) Chen, C.; Chen, Y.; Chuang, S. High-Performance and Highly Durable Inverted Organic Photovoltaics Embedding Solution-Processable Vanadium Oxides as an Interfacial Hole-Transporting Layer. *Adv. Mater. (Weinheim, Ger.)* **2011**, *23*, 3859−3863.
(32) Zilberberg, K.; Trost, S.; Schmidt, H.; Riedl, T. Solution Processed Vanadium Pentoxide as Charge Extraction Layer for Organic Solar Cells. *Adv. Energy Mater.* **2011**, *1*, 377−381.
(33) Zilberberg, K.; Trost, S.; Meyer, J.; Kahn, A.; Behrendt, A.; Lützenkirchen-Hecht, D.; Frahm, R.; Riedl, T. Inverted Organic Solar Cells with Sol−Gel Processed High Work-Function Vanadium Oxide Hole-Extraction Layers. *Adv. Funct. Mater.* **2011**, *21*, 4776−4783.
(34) Hancox, I.; Rochford, L. A.; Clare, D.; Walker, M.; Mudd, J. J.; Sullivan, P.; Schumann, S.; McConville, C. F.; Jones, T. S. Optimization of a High Work Function Solution Processed Vanadium Oxide Hole-Extracting Layer for Small Molecule and Polymer Organic Photovoltaic Cells. *J. Phys. Chem. C* **2013**, *117*, 49−57.
(35) Kim, J.; Kim, H.; Kim, G.; Back, H.; Lee, K. Soluble Transition Metal Oxide/Polymeric Acid Composites for Efficient Hole-Transport Layers in Polymer Solar Cells. *ACS Appl. Mater. Interfaces* **2014**, *6*, 951−957.
(36) Wang, F.; Sun, G.; Li, C.; Liu, J.; Hu, S.; Zheng, H.; Tan, Z.; Li, Y. Finding the Lost Open-Circuit Voltage in Polymer Solar Cells by UV-Ozone Treatment of the Nickel Acetate Anode Buffer Layer. *ACS Appl. Mater. Interfaces* **2014**, *6*, 9458−9465.
(37) Krishna, M.; Debauge, Y.; Bhattacharya, A. X-ray Photoelectron Spectroscopy and Spectral Transmittance Study of Stoichiometry in Sputtered Vanadium Oxide Films. *Thin Solid Films* **1998**, *312*, 116−122.
(38) Na, S.; Wang, G.; Kim, S.; Kim, T.; Oh, S.; Yu, B.; Lee, T.; Kim, D. Evolution of Nanomorphology and Anisotropic Conductivity in Solvent-Modified PEDOT:PSS Films for Polymeric Anodes of Polymer Solar Cells. *J. Mater. Chem.* **2009**, *19*, 9045−9053.
(39) Hou, J.; Chen, H.; Zhang, S.; Chen, R. I.; Yang, Y.; Wu, Y.; Li, G. Synthesis of a Low Band Gap Polymer and Its Application in Highly Efficient Polymer Solar Cells. *J. Am. Chem. Soc.* **2009**, *131*, 15586−15587.
(40) Tan, Z.; Zhang, W.; Zhang, Z.; Qian, D.; Huang, Y.; Hou, J.; Li, Y. High-Performance Inverted Polymer Solar Cells with Solution-Processed Titanium Chelate as Electron-Collecting Layer on ITO Electrode. *Adv. Mater. (Weinheim, Ger.)* **2012**, *24*, 1476−1481.
(41) He, K.; Yang, X.; Yan, H.; Wu, Z.; Li, Z.; Zhong, S.; Qu, Q.; Liang, R. Work Function Changes of Plasma Treated Indium Tin Oxide. *Org. Electron.* **2014**, *15*, 1731−1737.
(42) Meyer, J.; Shu, A.; Kroger, M.; Kahn, A. Effect of contamination on the electronic structure and hole-injection properties of semiconductor interfaces. *Appl. Phys. Lett.* **2010**, *96*, 133308.
(43) Zilberberg, K.; Gharbi, H.; Behrendt, A.; Trost, S.; Riedl, T. Low-Temperature, Solution-Processed MoO_x for Efficient and Stable Organic Solar Cells. *ACS Appl. Mater. Interfaces* **2012**, *4*, 1164−1168.
(44) Chen, M.; Wi, S.; Nam, H.; Priessnitz, G.; Liang, X. Block Copolymer Self Assembly for Design and Vapor-Phase Synthesis of Nanostructured Antireflective Surfaces. *J. Vac. Sci. Technol., B: Nanotechnol. Microelectron.: Mater., Process., Meas., Phenom.* **2014**, *32*, 06FF02.

DOI: 10.1021/acsami.5b00091
ACS Appl. Mater. Interfaces 2015, 7, 7613−7618